Journal of Materials Science and Engineering A 7 (9-10) (2017) 229-240
doi: 10.17265/2161-6213/2017.9-10.001

The Influence of Dehydration on the Electrical Conductivity of Trachyandesite at High Temperatures and High Pressures

Lidong Dai[1], Keshi Hui[1], Wenqing Sun[1,2], Haiying Hu[1], Heping Li[1] and Jianjun Jiang[1]

1. Key Laboratory of High-Temperature and High-Pressure Study of the Earth's Interior, Institute of Geochemistry, Chinese Academy of Sciences, Guiyang, Guizhou 550081, China

2. University of Chinese Academy of Sciences, Beijing 100039, China

Abstract: The electrical conductivity of trachyteandesite was measured in situ under conditions of pressure range from 0.5-2.0 GPa and temperature range from 773-1,323 K using a YJ-3000t multi-anvil press and a Solartron-1260 Impedance/Gain-phase Analyzer. The experimental results indicate that the electrical conductivity of trachyteandesite increases with increasing temperature and decreases with a rise in pressure. The relationship between the electrical conductivity (σ) and temperature (T) conforms to the Arrhenius equation within a certain temperature range. When the temperature rises to 923 K, the electrical conductivity of trachyandesite abruptly increases. This result demonstrates that trachyandesite begins to dehydrate at ~923 K and produces magnetite with a high-conductivity mineral phase after dehydration. The intergrowth of interconnected magnetite is the cause for the ~2 orders of magnitude increase in the electrical conductivity after dehydration. The interconnected high-conductivity mineral phase of magnetite in the dehydration product of the trachyandesite sample can be used to reasonably explain the high-conductivity anomalies in the South-Central Chilean subduction zone beneath the Andes.

Key words: High pressure, trachyandesite, electrical conductivity, dehydration, high-conductivity anomaly.

1. Introduction

Electrical conductivity is one of the most important parameters for providing constraints on the thermal structure and composition of the Earth's interior, and it is significant for studying the structure, electronic and ionic transport processes, defect chemistry, and other physical properties of minerals and rocks [1-6]. Consequently, it is extremely important for studying the electrical conductivities of the rocks that are widely distributed in the Earth's interior under appropriate thermodynamic conditions.

Trachyandesite, one of the most important andesitic rocks, stably exists as the transition rock between basaltic trachyandesite and trachyte trachydacite. Previous studies mainly focused on the electrical conductivities of trachyte protoliths and trachyte glass rather than fully considering a trachyandesite protolith [7-11]. Waff and Weill [7] measured the DC electrical conductivity of andesite with variations in the chemical composition under conditions of atmospheric pressure and different oxygen partial pressures, the results of which indicated that the effects of the alkali ion content of andesite are remarkable, whereas the iron content and oxygen fugacity have a relatively feeble influence on the electrical conductivity of a sample. Poe et al. [8] suggested that the transport process of pantelleritic trachyte glass is small polaron conduction at temperatures below 700 K and that ionic conduction becomes the main transport mechanism at temperatures higher than 973 K. In the ionic conduction regime, the electrical conductivity of the sample increased with increasing water content. Hui et

Corresponding author: Lidong Dai, full professor, research field: high pressure mineral physics.

al. [9] measured the grain interior and grain boundary conductivities of quartz andesite at temperatures below 973 K and proposed that the contribution of grain boundary conductivity to the total conductivity of quartz andesite continually decreases with increasing temperature and pressure. Laumonier et al. [10] measured the electrical conductivity of dacitic glass with different water contents (3.3-12.2 wt%) at conditions of 673-1,623 K and 0.15-3.0 GPa, and a functional relationship between temperature, pressure and water content was established. The relationship between the total conductivities of the grain boundaries and the grain interiors was obtained. Recently, Guo et al. [11] investigated the electrical conductivities of hydrous andesite melts with 0.01-5.9 wt% at 1,164-1,573 K and 0.5-1.0 GPa, and they found that the influence of water on the conductivities of andesitic melts is stronger than that for rhyolitic and dacitic melts. These authors proposed that the principal charge carrier was Na^+ in the anhydrous andesitic melt but that divalent cations were dominant in hydrous andesitic melts. As one of the most important volcanic rocks, trachyandesite is widely distributed throughout island-arc environments and might still occupy substantial space within the Earth's interior. In addition, systematic electrical conductivity measurements for trachyandesite at high temperatures and high pressures are crucial for understanding the physical properties of rocks in regional andesite-rich zones.

In this study, the electrical conductivity of trachyandesite was measured at pressures of 0.5-2.0 GPa and temperatures of 773-1,323 K in a frequency range of 10^{-1}-10^6 Hz. After dehydration, a series of characteristic parameters in the Arrhenius equation, including the pre-exponential factor and activation enthalpy, were acquired. The influence of dehydration on the electrical conductivity of the sample was also explored at a given temperature and pressure. Furthermore, we discussed the detailed geophysical implications of trachyandesite at high temperatures (T) and pressures (P).

2. Experimental Procedures

2.1 Sample Preparation

A sample of trachyandesite was collected from the town of Shizhu in the city of Yongkang, Zhejiang Province, China. The sample was fresh, non-fractured and nonoxidized, and it contained quartz, plagioclase and amphibole. To explore the chemical composition and corresponding mineralogical proportions, the sample was examined with an XRF (X-ray fluorescence) spectrometer, an electron microprobe analysis (EPMA) and an SEM (scanning electron microscope) at the State Key Laboratory of Ore Deposit Geochemistry, Institute of Geochemistry, Chinese Academy of Sciences, Guiyang, China. The TAS (total alkali and silica) classification of igneous rocks was used to confirm the precise name of the sample as trachyandesite (Fig. 1 and Table 1). From the representative optical microscope and back-scattered electron images, the main rock-forming minerals were determined to be plagioclase, amphibole and quartz phenocrysts, the corresponding volume ratios of which were approximately 50%, 30% and 20%, respectively, as shown in Fig. 2.

Before running the experiment, the trachyandesite was cut into cylinders of 6 mm in diameter and 6 mm

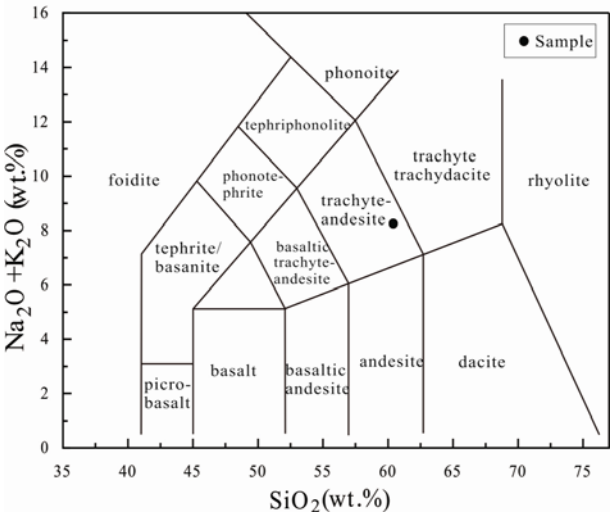

Fig. 1 TAS classification of igneous rocks.

Table 1 Chemical composition of whole rock analysis and main minerals of trachyandesite.

Oxides (wt%)	XRF for whole rock	EPMA for plagioclase	EPMA for amphibole
SiO_2	61.06	57.10	44.34
Al_2O_3	17.5	26.60	10.93
MgO	0.78	0.01	16.01
CaO	3.51	8.30	11.97
Na_2O	3.29	6.25	2.20
K_2O	4.94	0.80	0.76
FeO	4.78	0.29	8.70
TiO_2	0.69	0.01	1.26
Cr_2O_3	/	0.02	0.25
MnO_2	0.13	0.01	0.09
P_2O_5	0.20	/	/
L.O.I	2.94	/	/
Total	99.82	99.39	96.51

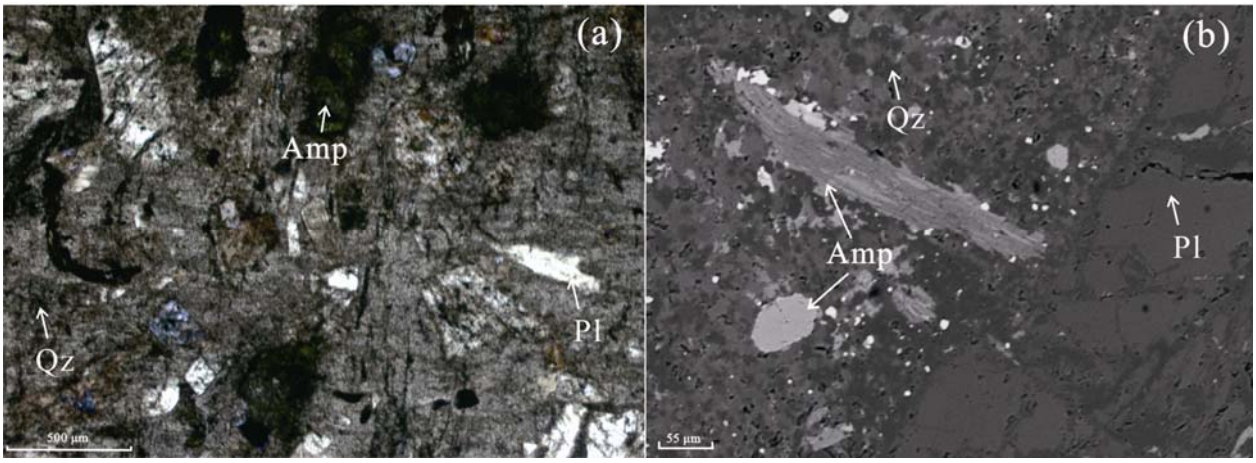

Fig. 2 Acquired representative photomicrographs (plane-polarized reflection) of light images and back-scattered electron images using a scanning electron microscope of the trachyandesite protolith before the electrical conductivity measurements. Abbreviations: plagioclase (*Pl*), amphibole (*Amp*) and quartz (*Qz*).

in height. The cylindrical samples were then cleaned in an ultrasonic cleaning device using deionized water, acetone and ethanol in turn. To avoid the influence of absorbed water on the conductivity measurements, all of the cylindrical samples were baked at 323 K for 12 h in an oven.

2.2 High-Pressure Cell and Impedance Measurements

The electrical conductivity measurements were carried out in a YJ-3000t multi-anvil apparatus and a Solartron-1260 Impedance/Gain-phase Analyzer at the Key Laboratory of High-Temperature and High-Pressure Study of the Earth's Interior, Institute of Geochemistry, Chinese Academy of Sciences. Detailed descriptions of the equipment and the experimental process can be found in previous studies conducted by Dai et al. [12, 13] and Hu et al. [14]. As shown in Fig. 3, a cubic pyrophyllite block (spec: 32.5 × 32.5 × 32.5 mm^3) was adopted as the pressure medium, and the heater was composed of three-layer stainless steel sheets (total thickness: 0.5 mm) in the shape of a tube. Alumina and magnesia sleeves were applied to ensure that the sample was in a relatively insulated environment, and 0.025-mm-thickness nickel foil was placed between the alumina and magnesia sleeves to shield the sample from external electromagnetic and spurious signal interference. The electrodes placed on the bottom and top of the sample

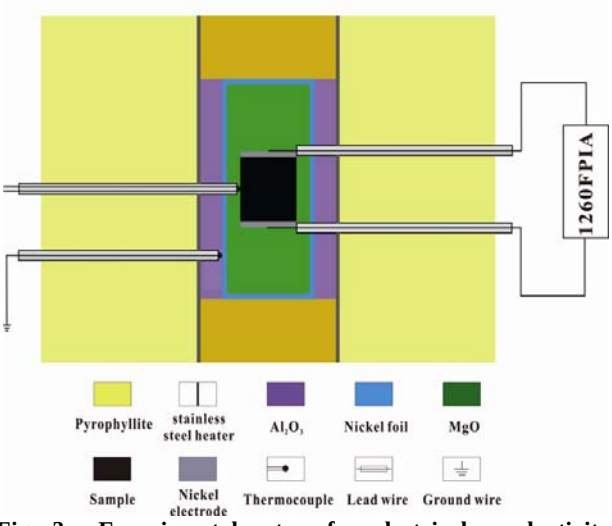

Fig. 3 Experimental setup for electrical conductivity measurements at high pressure.

were composed of two nickel disks (thickness: 0.5 mm; diameter: 6 mm). To avoid the influence of dehydration on the impedance spectroscopy measurements, all equipment, including the pyrophyllite and the alumina and magnesia sleeves, were heated at 1,173 K for 12 h in a muffle furnace. Their temperatures were monitored using a NiCr-NiAl thermocouple with a deviation of ±10 K.

During the experiments, the pressures were slowly raised at a speed of 1.0 GPa/h to the designed value. Then, under constant pressure conditions, the temperature was gradually increased at a rate of 100 K/h to the designated preset value in steps of 50-100 K. Once the temperature reached the desired value, a Solartron-1260 Impedance/Gain-phase Analyzer was operated to collect the impedance spectroscopy measurements with a sinusoidal signal voltage of 1.0 V in the frequency range of 10^{-1} to 10^{6} Hz. To ensure the reliability of the experimental results, the impedance spectra of the samples were measured several times at each temperature until the impedance arcs remained nearly unchanged.

3. Results

Nyquist and Bode diagrams of the complex impedance of trachyandesite under conditions of 1.5 GPa and 773-1,323 K in the frequency range of 10^{-1}-10^{6} Hz are shown in Figs. 4 and 5. As observed in Fig. 4, the semicircular diameters of the impedance arcs decrease rapidly as the temperature increases. Each semicircular impedance arc contains two parts, which correspond to different characteristic relaxation time constants. At high frequencies (~10^{2}-10^{6} Hz), one semicircular arc represents the conduction process of the grain interior, while the other part that appears at lower frequencies (~10^{-1}-10^{2} Hz) is related to the polarization process at the sample-electrode interface [15]. To ensure the precise fitting of the data and to acquire the conductivity results from the impedance spectra, we chose one equivalent circuit that was composed of the series connections R_S-C_S and R_E-C_E (R_S and C_S represent the resistance and capacitance of the bulk impedance for the sample, respectively; R_E and C_E represent the resistance and capacitance from the polarization effect of the sample-electrode interface,

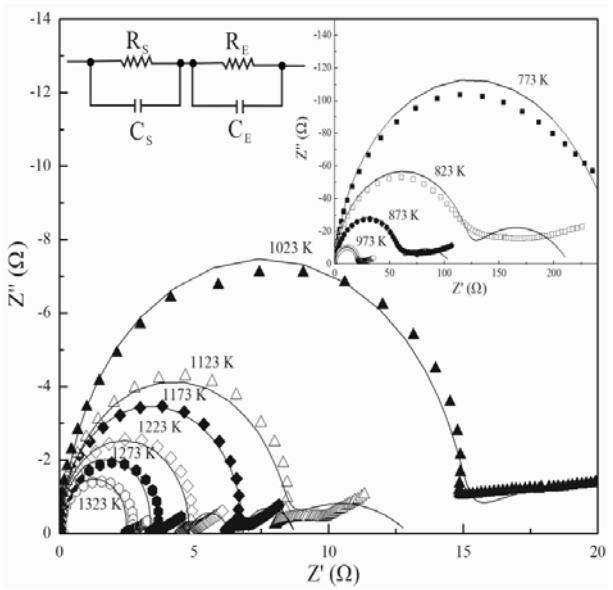

Fig. 4 Nyquist plane impedance of trachyandesite at frequencies from 10^{-1} to 10^{6} Hz (right to left) obtained under conditions of 1.5 GPa and 773-1,323 K. *Z'* and *Z''* are the real and imaginary parts of the complex impedance, respectively. The equivalent circuit that is composed of the series connections of R_S-C_S and R_E-C_E (R_S and C_S represent the resistance and capacitance of the bulk impedance for the sample, respectively; R_E and C_E represent the resistance and capacitance from the polarization effect of the sample-electrode interface, respectively) was selected to model the impedance semicircles.

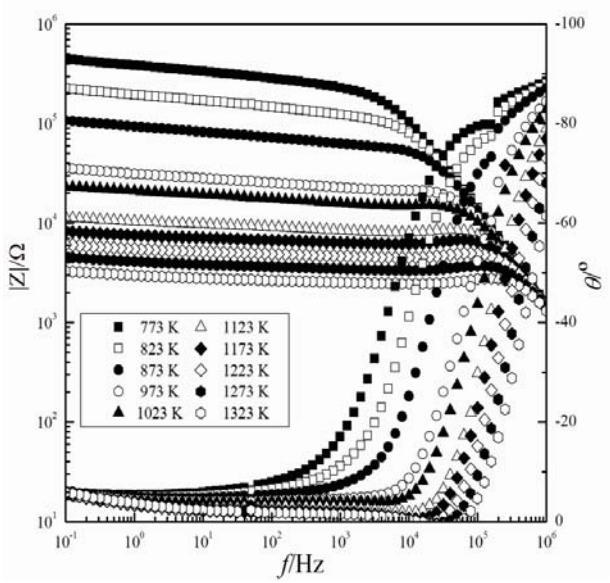

Fig. 5 Bode plane impedance of trachyandesite at frequencies from 10^{-1} to 10^{6} Hz under conditions of 1.5 GPa and 773-1323 K.

respectively) to model the semicircular impedance arcs and obtain the bulk resistance for the trachyandesite samples [16, 17]. In the Bode plane impedance of trachyandesite (Fig. 5), it is shown that the impedance modulus of the sample increases rapidly, and that the absolute value of the phase angle tends towards zero from high to low frequencies. According to impedance spectroscopy theory [18-21], the relationships between the real part (Z'), the imaginary part (Z''), the modulus ($|Z|$), and the phase angle (θ) are described as: $Z' = |Z| \cos\theta$ and $Z'' = |Z| \sin\theta$.

The bulk electrical conductivity of the sample is in accordance with the following expression:

$$\sigma = L / SR \quad (1)$$

where L is the sample length (m), S is the cross-sectional area of the electrode (m^2), and R is the resistance of the sample (Ω).

At pressures of 0.5-2.0 GPa and temperatures of 773-1,323 K, the relationship between the electrical conductivity of trachyandesite (σ) and the reciprocal of the temperature ($1/T$) was fitted using the Arrhenius equation:

$$\sigma = \sigma_0 \exp(-\Delta H / kT) \quad (2)$$

where σ_0 is the pre-exponential factor (S/m), ΔH is the activation enthalpy (eV), k is the Boltzmann constant, and T is the absolute temperature (K).

Fig. 6 shows the electrical conductivity of trachyandesite in the process of two heating and cooling cycles at a pressure of 2.0 GPa. In the first cycle, the electrical conductivity of trachyandesite slowly increases with an increase in the temperature up to 923 K and remarkably increases at temperatures higher than 923 K, which indicates that the dehydration reaction of trachyandesite occurs at 923 K under a given pressure of 2.0 GPa. After that, the electrical conductivity of the dehydration product of trachyandesite slowly continues to increase again. After the 1st heating cycle, the electrical conductivity of the dehydration product of trachyandesite displays a good repeatability in subsequent cycles. The influence of pressure on the electrical conductivity of the trachyandesite after dehydration in the temperature range of 773-1,323 K is illustrated in Fig. 7, and the fitted parameters of the Arrhenius equation are listed in Table 2. The electrical conductivity

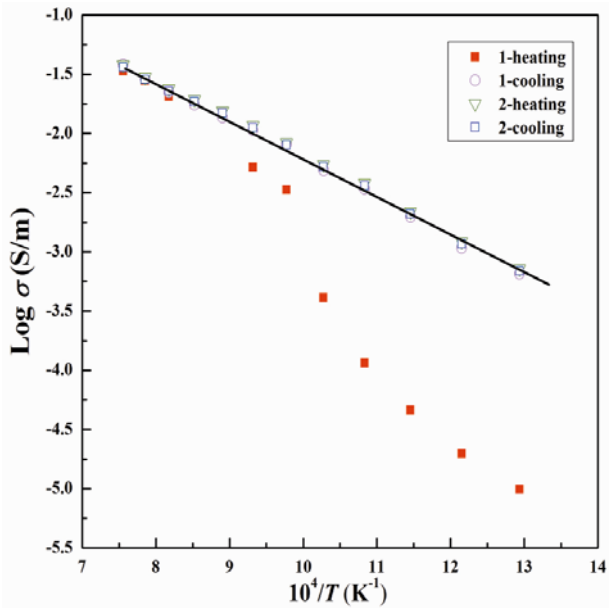

Fig. 6 Logarithm of the electrical conductivity versus the reciprocal of the temperature for trachyandesite in different heating/cooling cycles at 2.0 GPa. Data for the first heating cycle were excluded during the data fitting and analysis.

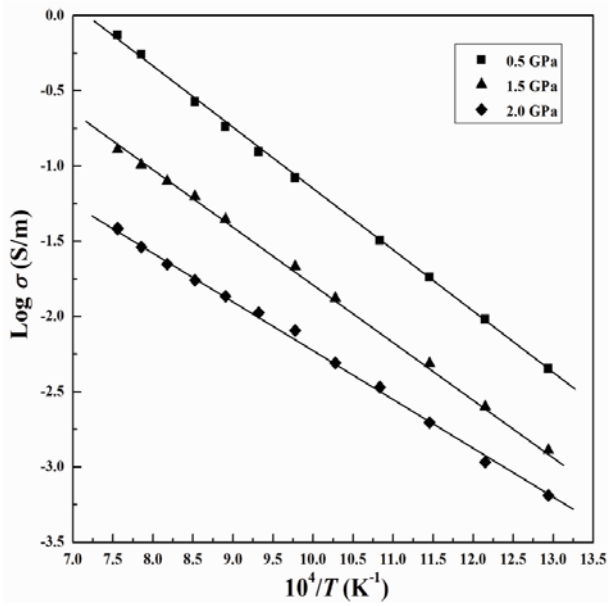

Fig. 7 Influence of pressure on the electrical conductivity of trachyandesite in the temperature range of 873-1173 K.

of the dehydration product of trachyandesite decreases with a rise in pressure, and the influence of pressure on the electrical conductivity is relatively weaker than that of temperature. Due to the occurrence of a dehydration reaction, we found that amphibole completely disappeared from the dehydration product of trachyandesite, which is illustrated in the back-scattered electron images of the recovered sample in Fig. 8. At the same time, amphibole is accompanied by some new mineral phase assemblages, including magnetite, quartz and pyroxene, which are formed simultaneously, as shown in Table 3.

4. Discussions

4.1 Comparison with Previous Studies

In the present study, we measured the electrical conductivity of trachyandesite and explored the influence of dehydration reactions on the electrical conductivity under pressure conditions in the range of 0.5-2.0 GPa and temperatures in the range of 773-1,323 K. After dehydration, the electrical conductivity of the sample decreased as the pressure rose, the activation enthalpy (ΔH) slightly decreased from 0.81 to 0.65 eV, and the logarithmic pre-exponential factor (Log σ_0) also decreased from 3.02 to 1.06. Dehydration reactions can greatly enhance

Table 2 Fitted parameters for electrical conductivity of trachyandesite.

Run No.	*P* (GPa)	*T* (K)	Log σ_0 (S/m)	ΔH (eV)	r^2
DH2	0.5-cooling	773-1,323	3.00 ± 0.04	0.80 ± 0.01	99.91
DH4	1.5-cooling	773-1,323	1.97 ± 0.07	0.74 ± 0.01	99.93
DH5	2.0-cooling	773-1,323	1.06 ± 0.04	0.65 ± 0.01	99.79
	2.0-heating	773-932	1.49 ± 0.49	0.99 ± 0.08	98.02

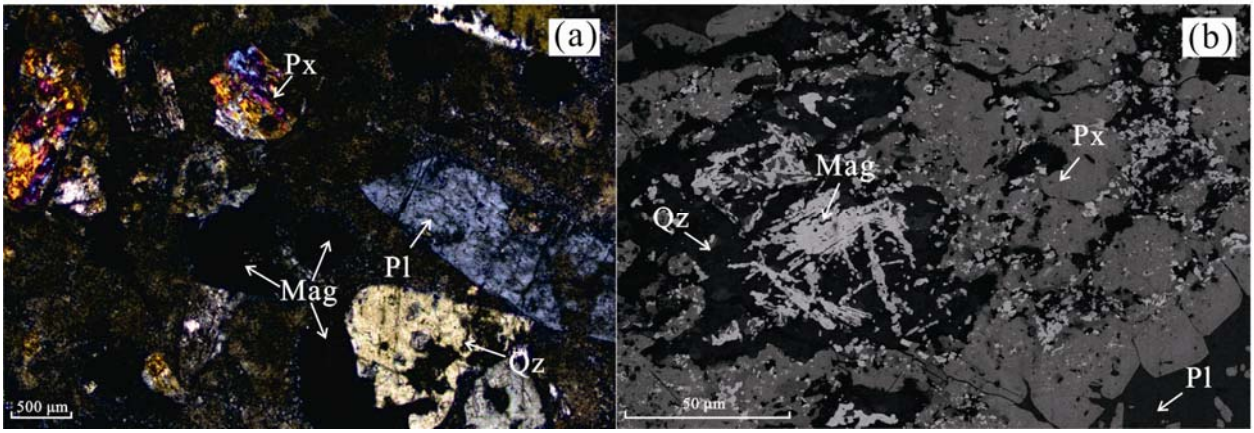

Fig. 8 Acquired representative photomicrographs (plane-polarized reflection) of light images and back-scattered electron images using a scanning electron microscope of the dehydration products for trachyandesite. Abbreviations: pyroxene (*Px*), plagioclase (Pl), quartz (Qz) and magnetite (Mag).

Table 3 Mineralogical assemblage of trachyandesite before and after dehydration. Amp = amphibole, Px = pyroxene, Pl = plagioclase, Qz = quartz and Mag = magnetite.

No.	*P* (GPa)	*T* (K)	Mineral associations
DH1	/	/	Amp (50%) + Pl (30%) + Qz (20%)
DH2	0.5	773-1,323	Px (35%) + Pl (30%) + Qz (20%) + Mag (15%)
DH3	1.5	773-1,323	Px (35%) + Pl (30%) + Qz (20%) + Mag (15%)
DH4	2.0	773-1,323	Px (35%) + Pl (30%) + Qz (20%) + Mag (15%)

the electrical conductivity with a profound effect on the electrical conductivity for water-bearing minerals and rocks in the subduction zone e.g., single crystal amphibole, brucite, serpentine, pyrophyllite, phlogopite, chloride, epidote, lawsonite, amphibolite, serpentinite, phyllite etc. [22-33]. Previous studies have already confirmed that the dehydration of single crystal amphibole and amphibole-bearing rocks occurs when temperatures exceed 873 K [23, 29]. In this study, the amphibole is the unique water-bearing mineral in our trachyandesite sample, and therefore, the dehydration of the rock originated from within the water-bearing amphibole. The observable dehydration temperature of trachyandesite (923 K) is very close to the results of previous studies [29]. The back-scattered electron images acquired using a scanning electron microscope for the recovered sample show that the dehydration reaction is sufficient and that all of the amphibole phenocrysts had thoroughly disappeared from the dehydration products, as is illustrated in Fig. 8 and Table 3. Accordingly, some new mineral phase assemblages, including pyroxene, quartz and some magnetite, appeared simultaneously, which were derived from the dehydration of amphibole. Notably, the interconnected magnetite (~15%) belongs to a representative high-conductivity mineral phase within the dehydration products of trachyandesite [34, 35]. Schmidbauer et al. [23] suggested that free water in amphibole cannot be produced during the dehydration process, the reaction equation of which can be described as follows:

$$Fe^{2+}+OH^{-} \rightarrow \frac{1}{2}H_2+O^{2-}+Fe^{3+} \quad (3)$$

The electrical conductivity of trachyandesite increases by nearly 2 orders of magnitude following dehydration. Interconnected magnetite is suggested to cause this remarkable enhancement of the conductivity for the dehydration product of the trachyandesite samples. Morris and Williams [36] found that the electrical conductivity of magnetite with a magnetic semiconductor increased by an order of magnitude owing to electron hopping between divalent and trivalent iron octahedral sites when the pressure rose from 0 to 20 GPa in a temperature range from 258 to 300 K. Kawano et al. [34] indicated that the electrical conductivity of synthesized serpentinite increases with an increase in the interconnected magnetite content during shear deformation and that the electrical conductivity of pure magnetite could reach nearly 10^3 S/m at 1.0 GPa and 750 K. Recently, Manthilake et al. [31] proposed that an interconnected network of a highly conductive and chemically impure magnetite mineral phase leads to an enhancement of the electrical conductivity for hydrous chlorite up to 7×10^{-1} S/m after dehydration upon heating to 923 K at the pressure of respective 2.0 GPa and 4.0 GPa. Based on these obtained conductivity results for hydrous chloride, the authors found that the dehydration of chloride could be used to reasonably explain high-conductivity anomalies (~1 S/m) in the mantle wedge zone. Therefore, in the present study, it is suggested that the intergrowth of interconnected magnetite causes the remarkable increase in electrical conductivity for hydrous trachyandesite after dehydration.

On the other hand, upon considering our new results regarding the influence of pressure on the electrical conductivity of trachyandesite, we compared our data with those from previous studies [7-11], as

shown in Fig. 9. The influence of the alkali ion content (4.96-7.83 wt%), iron content and oxygen fugacity on the DC electrical conductivity of andesite was determined by Waff and Weill [7] at atmospheric pressure and high temperatures. In a comprehensive consideration of the differences in the alkali ion content (3.29 wt% Na_2O in our trachyandesite sample and 4.96 wt% from Ref. [7]), the chemical composition effects and the method employed, there exists a good consistency in the electrical conductivities for andesite with those of our results. The previous results for andesites were measured using AC impedance spectroscopy techniques to obtain the electrical conductivities of trachyte protoliths and trachyte glass, including hydrous and anhydrous pantelleritic trachyte glass from Ref. [8], quartz andesite from Ref. [9], and dacitic glass with different water contents (3.3-12.2 wt%) from Ref. [10], which are consistent with our electrical conductivities for trachyandesite protoliths. Recently, Guo et al. [11]

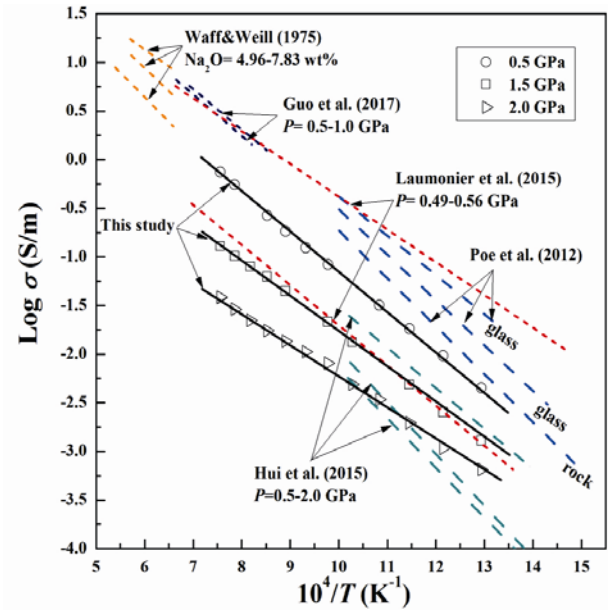

Fig. 9 Comparison of the results from this study at pressures of 0.5-2.0 GPa (black solid lines) with those of previous studies for the electrical conductivities of trachyandesite. The broken dashed and dotted yellow, blue, red, green and violet lines represent the electrical conductivities of trachyte protoliths and trachyte from Refs. [7-11], respectively.

investigated the electrical conductivities of hydrous andesite melts with 0.01-5.9 wt% water contents at 1,164-1,573 K and 0.5-1.0 GPa, which revealed some obvious discrepancies due to variations in the chemical composition, melting fractions and water contents in the experimental products at high-temperature conditions.

4.2 Implications

The Andes Mountains are located along the active edge of the South American Plate, and a large quantity of andesites is widespread throughout the middle-lower crust beneath the Andes. Previous geomagnetic and magnetotelluric sounding results have indicated that many high-conductivity layers exist in the middle-lower crust beneath the Andes [37-42]. Combining in situ laboratory conductivity measurements from high-pressure experiments with field magnetotelluric data is crucial to reveal the cause for these highly conductivity layers. There are abundant volcanic rocks in the vicinity of the Andes, and magma deposits in active volcanic environments have been proposed to cause highly conductive zones beneath volcanic arcs [41, 42]. However, another potential and crucial candidate for the explanation of such high-conductivity zones is the dehydration of hydrous minerals and rocks in the middle-lower crust beneath the Andes and the associated subduction zone. Therefore, it is valuable to investigate whether the dehydration of trachyandesite can cause the formation of highly conductive layers.

We applied the electrical conductivities for the dehydration products of trachyandesite to establish a laboratory-based conductivity-depth profile. The corresponding profile for the middle-lower crust of the southern Andes can be constructed by converting the conductivity-temperature data into conductivity-depth results in combination with the parameters we determined in this study using the Arrhenius Eq. (2) under pressures of 0.5-2.0 GPa. The relationship between temperature and depth for stationary

continental crust can be described by the numerical solution of the heat conduction equation [43]:

$$T = T_0 + (\frac{Q}{k})z - (\frac{A_0}{2k})z^2 \quad (4)$$

where T_0 is the surface temperature (K), Q is the surface heat flow (mW/m^2), z is the lithospheric layer depth (km), k is the thermal conductivity (W/mK), and A_0 is the lithospheric radiogenic heat productivity (μW/m^3). Previous results suggested parameter values for the lithospheric radiogenic heat productivity (A_0) and the thermal conductivity (k) of 0.31 μW/m^3 and 2.6 W/mK, respectively [44]. In consideration of field magnetotelluric data (38-41°S and 71-74 W) from the coastline of the South-Central Chilean subduction zone beneath the Andes, a few discontinuous high-conductivity zones have been discovered at depths of 20-40 km, and the Moho is located at a depth of nearly 40 km in this area. The magnetotelluric results on the South-Central Chilean subduction zone beneath the Andes obtained by Ref. [42] are included in Fig. 10.

Previous studies reported surface heat flow values for the Arauco basin of South-Central Chile (37-38°S) and the central Andes (28-30°S) are 33-51 mW/m^2 and 64 ± 4 mW/m^2, respectively [45, 46]. Using Eq. (4), the relationship between the electrical conductivity of trachyandesite and depth at pressures of 0.5-2.0 GPa is shown in Fig. 10. The electrical conductivity of trachyandesite at depths of 20-40 km is obviously lower than that in the high-conductivity zone when the lower boundary of surface heat flow is 33 mW/m^2. Therefore, the data obtained here cannot reasonably explain the anomalies observed in the South-Central Chilean subduction zone beneath the Andes. Using the upper boundary of surface heat flow from the Arauco basin of the central Andes (64 mW/m^2), the electrical conductivity of trachyandesite at 0.5 GPa is similar to the values of the highest conductivity of the high-conductivity zone, which can be used to explain the high-conductivity

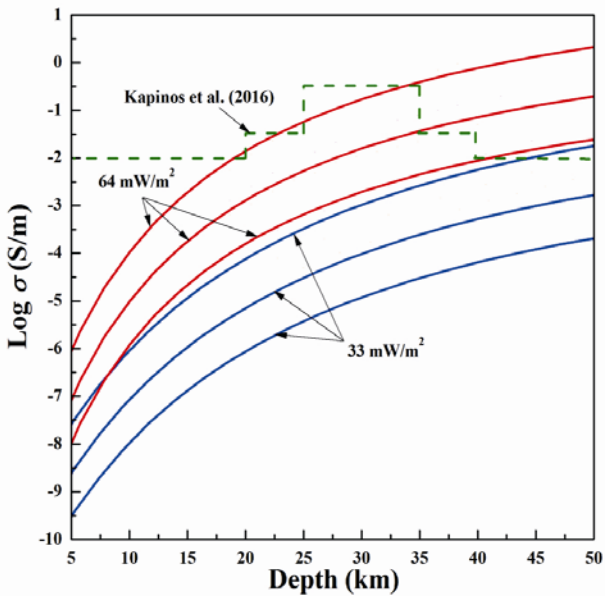

Fig. 10 Two sets of laboratory-based conductivity-depth profiles as functions of different pressures compared with the magnetotelluric field results for the anomalous high-conductivity zones in the South-Central Chilean subduction zone beneath the Andes. The solid blue and red lines indicate the laboratory-based conductivity-depth profiles for trachyandesite are based on heat flow values of 33 and 64 mW/m^2 for the lower and upper boundaries of the Andes in the Arauco basin of South-Central Chile and the central Andes, respectively. The broken green line denotes the high-conductivity anomalies beneath the high-conductivity zones of the South-Central Chilean subduction zone beneath the Andes at depths of 25-35 km [42].

anomaly in this area. However, the results at 1.5-2.0 GPa are nearly one order of magnitude lower than the data from the high-conductivity zone, which implies that it is not easy to evaluate whether the high-conductivity anomaly in the South-Central Chilean subduction zone beneath the Andes is caused by the dehydration product of trachyandesite. Of course, our results make it clear that magnetite content can play a crucial role in the electrical conductivity of the dehydration product of trachyandesite, and thus, the trachyandesite with various amphibole contents may result in different electrical conductivity values for the products of trachyandesite after dehydration. In conclusion, the interconnected high-conductivity mineral phase of magnetite in the dehydration product

of the trachyandesite sample can be used to reasonably explain the high-conductivity anomalies in the South-Central Chilean subduction zone beneath the Andes.

5. Conclusions

The electrical conductivity of trachyandesite was measured under the conditions of 0.5-2.0 GPa and 773-1,323 K. The electrical conductivity of trachyandesite increases by nearly 2 orders magnitude following the dehydration of the sample. After dehydration, the electrical conductivity of trachyandesite increases with increasing temperature and decreases with a rise in pressure. The intergrowth of interconnected Magnetite in the dehydration product is the most plausible reason for the high-conductivity anomalies for the South-Central Chilean subduction zone beneath the Andes.

Acknowledgments

We appreciate Dr. Aaron Stallard in Stallard Scientific Editing Company for their help in English language improvements of the manuscript. This research was financially supported by the Strategic Priority Research Program (B) of the Chinese Academy of Sciences (XDB 18010401), Key Research Program of Frontier Sciences of CAS (QYZDB-SSW-DQC009), "135" Program of the Institute of Geochemistry of CAS, Hundred Talents Program of CAS and NSF of China (41474078, 41774099 and 41772042).

References

[1] Hirsch, L. M., Shankland, T. J., and Duba, A. G. 1993. "Electrical Conduction and Polaron Mobility in Fe-Bearing Olivine." *Geophysical Journal International* 114: 36-44.

[2] Nover, G. 2005. "Electrical Properties of Crustal and Mantle Rocks—A Review of Laboratory Measurements and Their Explanation." *Surveys in Geophysics* 26: 593-651.

[3] Dai, L., Li, H., Hu, H., Shan, S., Jiang, J., and Hui, K. 2012. "The Effect of Chemical Composition and Oxygen Fugacity on the Electrical Conductivity of Dry and Hydrous Garnet at High Temperatures and Pressures." *Contributions to Mineralogy and Petrology* 163: 689-700.

[4] Dai, L., Hu, H., Li, H., Jiang, J., and Hui, K. 2014. "Effects of Temperature, Pressure and Chemical Composition on the Electrical Conductivity of Granite and Its Geophysical Implications." *American Mineralogist* 99: 1420-8.

[5] Ferri, F., Gibert, B., Violay, M., and Cesare, B. 2013. "Electrical Conductivity in a Partially Molten Crust From Measurements on Metasedimentary Enclaves." *Tectonophysics* 586: 84-94.

[6] Hu, H., Dai, L., Li, H., Hui, K., and Li, J. 2015. "Temperature and Pressure Dependence of Electrical Conductivity in Synthetic Anorthite." *Solid State Ionics* 276: 136-41.

[7] Waff, H. S., and Weill, D. F. 1975. "Electrical Conductivity of Magmatic Liquids: Effects of Temperature, Oxygen Fugacity and Composition." *Earth and Planetary Science Letters* 28: 254-60.

[8] Poe, B. T., Romano, C., Di Genova, D., Behrens, H., and Scarlato, P. 2012. "Mixed Electrical Conduction in a Hydrous Pantellerite Glass." *Chemical Geology* 320-1: 140-6.

[9] Hui, K., Zhang, H., Li, H., Dai, L., Hu, H., Jiang, J., and Sun, W. 2015. "Experimental Study on the Electrical Conductivity of Quartz Andesite at High Temperature and High Pressure: Evidence of Grain Boundary Transport." *Solid Earth* 6: 1037-43.

[10] Laumonier, M., Gaillard, F., and Sifre, D. 2015. "The Effect of Pressure and Water Concentration on the Electrical Conductivity of Dacitic Melts: Implication for Magnetotelluric Imaging in Subduction Areas." *Chemical Geology* 418: 66-76.

[11] Guo, X., Li, B., Ni, H., and Mao, Z. 2017. "Electrical Conductivity of Hydrous Andesitic Melts Pertinent to Subduction Zones." *Journal of Geophysical Research: Solid Earth* 122: 1777-88.

[12] Dai, L., Li, H., Hu, H., and Shan, S. 2008. "Experimental Study of Grain Boundary Electrical Conductivities of Dry Synthetic Peridotite under High-Temperature, High-Pressure, and Different Oxygen Fugacity Conditions." *Journal of Geophysical Research: Solid Earth* 113: B12211.

[13] Dai, L., Hu, H., Li, H., Wu, L., Hui, K., Jiang, J., and Sun, W. 2016. "Influence of Temperature, Pressure, and Oxygen Fugacity on the Electrical Conductivity of Dry Eclogite, and Geophysical Implications." *Geochemistry, Geophysics, Geosystems* 17: 2394-407.

[14] Hu, H., Li, H., Dai, L., Shan, S., and Zhu, C. 2011. "Electrical Conductivity of Albite at High Temperatures and High Pressures." *American Mineralogist* 96: 1821-7.

[15] Roberts, J. J., and Tyburczy, J. A. 1991. "Frequency Dependent Electrical Properties Of Polycrystalline Olivine Compacts." *Journal of Geophysical Research: Solid Earth* 96: 16205-22.

[16] Saltas, V., Chatzistamou, V., Pentari, D., Paris, E., Triantis, D., Fitilis, I., and Vallianatos, F. 2013. "Complex Electrical Conductivity Measurements of a KTB Amphibolite Sample at Elevated Temperatures." *Materials Chemistry and Physics* 139: 169-75.

[17] Saltas, V., Fitilis, I., and Vallianatos, F. 2014. "A Combined Complex Electrical Impedance and Acoustic Emission Study in Limestone Samples Under Uniaxial Loading." *Tectonophysics* 637: 198-206.

[18] Nover, G., Will, G., and Waitz, R. 1992. "Pressure Induced Phase Transition in Mg_2GeO_4 as Determined by Frequency Dependent Complex Electrical Resistivity Measurements." *Physics and Chemistry of Minerals* 19: 133-9.

[19] Huebner, J. S., and Dillenburg, R. G. 1995. "Impedance Spectra of Hot, Dry Silicate Minerals and Rock: Qualitative Interpretation of Spectra." *American Mineralogist* 80: 46-64.

[20] Dai, L., Li, H., Hu, H., Jiang, J., Hui, K., and Shan, S. 2013. "Electrical Conductivity of $Alm_{82}Py_{15}Grs_3$ Almandine-Rich Garnet Determined by Impedance Spectroscopy at High Temperatures and High Pressures." *Tectonophysics* 608: 1086-93.

[21] Dai, L., Hu, H., Li, H., Hui, K., Jiang, J., Li, J., and Sun, W. 2015. "Electrical Conductivity of Gabbro: The Effects of Temperature, Pressure and Oxygen Fugacity." *European Journal of Mineralogy* 27: 215-24.

[22] Hicks, T., and Secco T. 1997. "Dehydration and Decomposition of Pyrophyllite at High Pressures: Electrical Conductivity and X-Ray Diffraction Studies to 5 Gpa." *Canadian Journal of Earth Sciences* 34: 875-82.

[23] Schmidbauer, E., Kunzmann, T., Fehr, T., and Hochleitner, R. 2000. "Electrical Resistivity and 57Fe Mossbauer Spectra Of Fe-Bearing Calcic Amphiboles." *Physics and Chemistry of Minerals* 27: 347-56.

[24] Xie, H., Zhou, W., Zhu, M., and Liu, Y. 2002. "Elastic and Electrical Properties of Serpentinite Dehydration at High Temperature and High Pressure." *Journal of Physics: Condensed Matter* 14: 11359-63.

[25] Popp, R. K., Hibbert, H. A., and Lamb, W. M. 2006. "Oxy-Amphibole Equilibria in Ti-Bearing Calcic Amphiboles: Experimental Investigation and Petrologic Implications for Mantle-Derived Amphiboles." *American Mineralogist* 91: 54-66.

[26] Ter Heege, J. H., and Renner, J. 2007. "In Situ Impedance Spectroscopy on Pyrophyllite and $CaCO_3$ at High Pressure and Temperature: Phase Transformations and Kinetics of Atomistic Transport." *Physics and Chemistry of Minerals* 34: 445-65.

[27] Gasc, J., Brunet, F., Bagdassarov, N., and Morales-Flórez, V. 2011. "Electrical Conductivity of Polycrystalline $Mg(OH)_2$ at 2 Gpa: Effect of Grain Boundary Hydration-Dehydration." P*hysics and Chemistry of Minerals* 38: 543-56.

[28] Reynard, B., Mibe, K., and de Moortèle, B. V. 2011. "Electrical Conductivity of the Serpentinised Mantle and Fluid Flow in Subduction Zones." *Earth and Planetary Science Letters* 307: 387-94.

[29] Wang, D., Guo, Y., Yu, Y., and Karato, S.-I. 2012. "Electrical Conductivity of Amphibole-Bearing Rocks: Influence of Dehydration." *Contributions to Mineralogy and Petrology* 164: 17-25.

[30] Manthilake, G., Mookherjee, M., Bolfan-Casanova, N., and Andrault, D. 2015. "Electrical Conductivity of Lawsonite and Dehydrating Fluids at High Pressures and Temperatures." *Geophysical Research Letters* 42: 7398-405.

[31] Manthilake, G., Bolfan-Casanova, N., Novella, D., Mookherjee, M., and Andrault, D. 2016. "Dehydration of Chlorite Explains Anomalously High Electrical Conductivity in the Mantle Wedges." *Science Advances* 2: e1501631.

[32] Li, Y., Yang, X., Yu, J., and Cai, Y. 2016. "Unusually High Electrical Conductivity of Phlogopite: The Possible Role of Fluorine and Geophysical Implications." *Contributions to Mineralogy and Petrology* 171: 37.

[33] Hu, H., Dai, L., Li, H., Hui, K., and Sun, W. 2017. "Influence of Dehydration on the Electrical Conductivity of Epidote and Implications for High-Conductivity Anomalies in Subduction Zones." *Journal of Geophysical Research: Solid Earth* 122: 2751-62.

[34] Kawano, S., Yoshino, T., and Katayama, I. 2012. "Electrical Conductivity of Magnetite-Bearing Serpentinite during Shear Deformation." *Geophysical Research Letters* 39: L20313.

[35] Ferreira, N. M., Kovalevsky, A. V., Naumovich, E. N., Yaremchenko, A. A., Zakharchuk, K. V., Costa, F. M., and Frade, J. R. 2014. "Effects of Transition Metal Additives on Redox Stability and High-Temperature Electrical Conductivity of $(Fe,Mg)_3O_4$ Spinels." *Journal of the European Ceramic Society* 34: 2339-50.

[36] Morris, E. R., and Williams, Q. 1997. "Electrical Resistivity of Fe_3O_4 to 48 Gpa: Compression-Induced Changes in Electron Hopping at Mantle Pressures." *Journal of Geophysical Research: Solid Earth* 102: 18139-48.

[37] Schilling, F. R., Partzsch, G. M., Brasse, H., and Schwarz, G. 1997. "Partial Melting Below the Magmatic Arc in the Central Andes Deduced from Geoelectromagnetic Field Experiments and Laboratory Data." *Physics of the Earth*

and Planetary Interiors 103: 17-31.

[38] Schmitz, M., Heinsohn, W. D., and Schilling, F. R. 1997. "Seismic, Gravity and Petrological Evidence for Partial Melt Beneath the Thickened Central Andean Crust (21-23°S)." *Tectonophysics* 270: 313-26.

[39] Partzsch, G. M., Schilling, F. R., and Arndt, J. 2000. "The Influence of Partial Melting on the Electrical Behavior of Crustal Rocks: Laboratory Examinations, Model Calculations and Geological Interpretations." *Tectonophysics* 317: 189-203.

[40] Schilling, F. R., and Partzsch, G. M. 2001. "Quantifying Partial Melt Fraction in the Crust Beneath the Central Andes and the Tibetan Plateau." *Physics and Chemistry of the Earth, Part A: Solid Earth and Geodesy* 26: 239-46.

[41] García, K., and Díaz, D. 2016. "Three-Dimensional Geo-Electrical Structure in Juncalito Geothermal Prospect, Northern Chile." *Geothermics* 64: 527-37.

[42] Kapinos, G., Montahaei, M., Meqbel, N., and Brasse, H. 2016. "Three-Dimensional Electrical Resistivity Image of the South-Central Chilean Subduction Zone." *Tectonophysics* 666: 76-89.

[43] Čermák, V., and Laštovičková, M. 1987. "Temperature Profiles in the Earth of Importance to Deep Electrical Conductivity Models." *Pure and Applied Geophysics* 125: 255-84.

[44] Zhou, W., Fan, D., Liu, Y., and Xie, H. 2011. "Measurements of Wave Velocity and Electrical Conductivity of an Amphibolite from Southwestern Margin of the Tarim Basin at Pressures to 1.0 Gpa and Temperatures to 700 °C: Comparison with Field Observations." *Geophysical Journal International* 187: 1393-404.

[45] Kuhn, P. P., Echtler, H., Littke, R., and Alfaro, G. 2010. "Thermal Basin Modelling of the Arauco Forearc Basin, South Central Chile-Heat Flow and Active Margin Tectonics." *Tectonophysics* 495: 111-28.

[46] Collo, G., Dávila, F. M., Nóbile, J., Astini, R. A., and Gehrels, G. 2011. "Clay Mineralogy and Thermal History of the Neogene Vinchina Basin, Central Andes of Argentina: Analysis of Factors Controlling the Heating Conditions." *Tectonics* 12(30): 386-94.